Low Temperature Physics/Fizika Nizkikh Temperatur, 2021, vol. 47, No. 10, pp. 928–937

Magnetoresistance of graphite nanoplatelets with different structure

I. V. Ovsiienko, T. A. Len, O. A. Syvolozhskyy, and L. Yu. Matzui

Taras Shevchenko National University of Kyiv, Kyiv 01601, Ukraine
E-mail: ovsiienko@univ.kiev.ua

I. G. Mirzoiev, V. V. Andrievskii, and E. Yu. Beliayev

B. Verkin Institute for Low Temperature Physics and Engineering of the National Academy of Sciences of Ukraine
Kharkiv 61103, Ukraine

Received April 21, 2021, revised May 26, 2021, published online August 26, 2021

The magnetoresistance of bulk specimens of graphite nanoplatelets obtained by different methods is studied in magnetic fields up to 2.2 T. It has been established that magnetoresistance is negative for graphite nanoplatelets prepared by chemical treatment of source graphite with a solution of potassium permanganate in sulfuric acid. This negative magnetoresistance can be explained in terms of the model of charge carrier's weak localization in a system with imperfect structure. It has been established that the magnetoresistance is positive and independent of temperature for graphite nanoplatelets produced by sonication method. Moreover, magnetoresistance is linear relative to a magnetic field in fields above ~ 0.7 T. It is shown that linear magnetoresistance can be explained in the terms of the Abrikosov's model of quantum linear magnetoresistance.

Keywords: graphite nanoplatelets, magnetoresistance, structure imperfection, weak localization, quantum magnetoresistance.

1. Introduction

In recent years, there has been a growing interest in structures based on nanographite and nanocarbon, which exhibit a wide range of unique properties, such as transport properties, mechanical, optical, and others. The electron transport properties of graphite materials have been studied quite well. But as for the properties of nanographite and graphene-like structures, there are still many open questions. In particular, the most common methods of obtaining graphite nanoplatelets and graphene-like structures are that the source graphite materials are treated with strong oxidants and/or ultrasound. And it is obvious that such treatment can cause both a weakening of the interaction between the graphene layers and a partial destruction of the graphene layers structure itself. That, in turn, results into a change in all the properties of graphene materials, in particular, transport properties.

Among the charge transport properties, which are very sensitive to changes in the graphite particle dimensions and degree of their defectiveness, we can highlight the conductivity in the magnetic field. Magnetoresistance or the relative change of electrical resistance in a magnetic field for monocrystalline natural graphite has been studied very well. Sufficiently perfect crystals of pure natural graphite are characterized by a positive magnetoresistance, which quadratically depends on the magnetic field. At low temperatures, the magnetoresistance increases and can reach very large values up to 1000 %. This increase in magnetoresistance is due to the growth of the charge carrier's mobility with decreasing temperature. Thus, the temperature dependence of magnetoresistance of perfect natural monocrystalline graphite indicates a significant contribution of phonons in the scattering mechanisms of current carriers. However, even a slight increase in the defectiveness of the graphite structure changes the mechanisms of the magnetoresistance and, as a consequence, causes a change in the temperature dependence of the magnetoresistance. As a result, for fine crystalline and polycrystalline graphite as well as for soft carbons and pregraphite carbons, [1–6] the negative magnetoresistance is usually observed. Most authors explain this negative magnetoresistance in graphite materials with an imperfect structure by the manifestation of the quantum effect of the charge carriers' weak localization. In this case graphite materials are considered as 3D systems [7–9].

There are a significant number of works in which the authors found anomalous temperature and field dependences of the magnetoresistance for graphene-like structures and graphites with a small degree of defectiveness. In the papers [10–13], results of magnetoresistance studies in multilayered epitaxial graphene are presented. It was found that a linear relative to the magnetic field magnetoresistance is observed for multilayered epitaxial graphene, which reaches 80 % at room temperature. However, the authors did not agree on whether the obtained results should be explained within the classical linear magnetoresistance model or a quantum linear magnetoresistance. In [14], both the positive and negative linear magnetoresistance is revealed depending on the structural perfection for bulk graphite with different particle sizes.

In this paper, we present the results of magnetoresistance studies in bulk specimens of graphite nanoplatelets (GNPs) obtained by different methods, particularly by the method of chemical treatment with strong oxidants and by the sonication method.

2. Experimental

2.1. Obtaining nanographite specimens

For investigations of transport properties, several specimens of GNPs with different structures have been prepared. As a source for obtaining GNPs specimens, thermoexfoliated graphite (TEG) has been used. For obtaining TEG, natural dispersed graphite of Zavalivskyy deposit (GAK–1) was intercalated with sulfuric acid by the bichromatic method up to the first stage, and then it was subjected to thermal exfoliation in the temperature interval of 1173–1273 K in an upstream furnace. This method for obtaining of TEG is described in detail in [15].

Two methods were used to obtain the GNP specimens: chemical treatment of source TEG (specimen #1) and sonication of source TEG in different mediums (specimens #2 – #4). For the preparation of specimen #1 source TEG was treated by 1.5 M solution of $KMnO_4$ in sulfuric acid. At the first stage, a TEG powder was placed in a conical flask and filled with the solution of $KMnO_4$ in H_2SO_4. Then the suspension was dispersed in a magnetic stirrer for 1 h and boiled for 5 h. Then TEG was impregnated for 24 h and re-dispersed in a magnetic stirrer. At the last stage, the suspension was filtrated and obtained GNPs powder was washed with a distilled deionized water to remove sediment until neutral pH and dried at 390 K till constant mass (~ 8 h). For obtaining the GNP specimens by the sonication method, the source TEG was subjected to ultrasonic dispersion in various media, in ethanol (specimen #2, sonication time is 1.5 h), in acetone (specimen #3, sonication time is 3 h) and in water (specimen #4, sonication time is 20 h).

The powders of rich black color with a pronounced metallic shine have been obtained after applying the chemical treatment and sonication methods to the source TEG. The bulk density of the obtained powders is approximately ten times greater than the bulk density of the source TEG. The increase in the bulk density of the GNPs powders is apparently due to the destruction of the "worm-like" loose structure of the source TEG particles during the chemical and ultrasonic treatment. The presence of metallic shine in nanographite particles indirectly indicates that in the process of chemical or ultrasonic treatment of the source TEG there is a destruction of loose bulk particles of the TEG along the direction of the graphite planes into individual graphite sheets. In this process, the sheet surface defectiveness does not change or changes very little, giving the powder a metallic shine inherent to perfect fine-crystalline graphite.

2.2. Structure of graphite nanoplatelets obtained with different methods

According to x-ray diffraction data for all specimens of GNPs, the distance d_{002} between neighboring layers is 0.336 nm. In more detail, the structure of obtained graphite nanoplatelets has been studied with electron microscopy, including high-resolution electron microscopy (electron microscope JEOL 200). The fragments of electron microscopy images of nanographite specimens #1 and #3 are presented in Fig. 1.

As can be seen from Fig. 1, for specimen #1, the crystalline size (defect-free region) is estimated as $L_a \sim 5$ nm, and for specimen #3 $L_a \sim 40$ nm.

The Raman spectroscopy method was used for a more detailed determination of the degree of defectiveness of

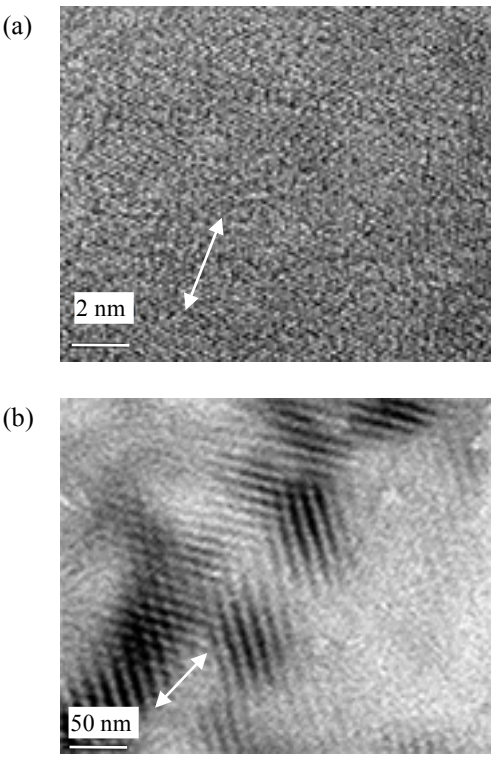

Fig. 1. The fragments of electron microscopy images of GNPs specimens #1 (a) and #3 (b).

nanographite sheets (Horiba LabRAM ARAMIS Raman spectrometer). Fig. 2 presents the Raman spectra for source TEG and for GNPs obtained. Some parameters of Raman spectra, such as a position of the G band (x_G) and half-width of G band (w_G), the ratio of integral intensities of G band and D band (A_G/A_D), positions of the overtones of D band (G_1' and G_2') also are presented in Table 1.

Table 1. The results of profile analysis for the Raman spectra of the source TEG and GNPs

Sample	x_D, cm^{-1}	x_G, cm^{-1}	w_G, cm^{-1}	A_G/A_D	$x_{G_1'}$, cm^{-1}	$x_{G_2'}$, cm^{-1}
TEG	1351	1580.0	14.31	11.11	2685	2722
#1	1350.4	1580.7	18.94	6.70	2692	2723
#2	1349	1580.5	15.4	5.55	2687	2721
#3	1353.8	1580.5	15.03	11.11	2686	2722
#4	1349	1580.4	14.6	9.03	2685	2721

As shown in Fig. 2, the Raman spectra for source TEG and obtained GNPs are similar. The Raman spectra for all specimens contain intensive G band assigned to the in-plane vibration of the C–C bond, weakly intensive D band activated by the presence of disorder in the carbon systems

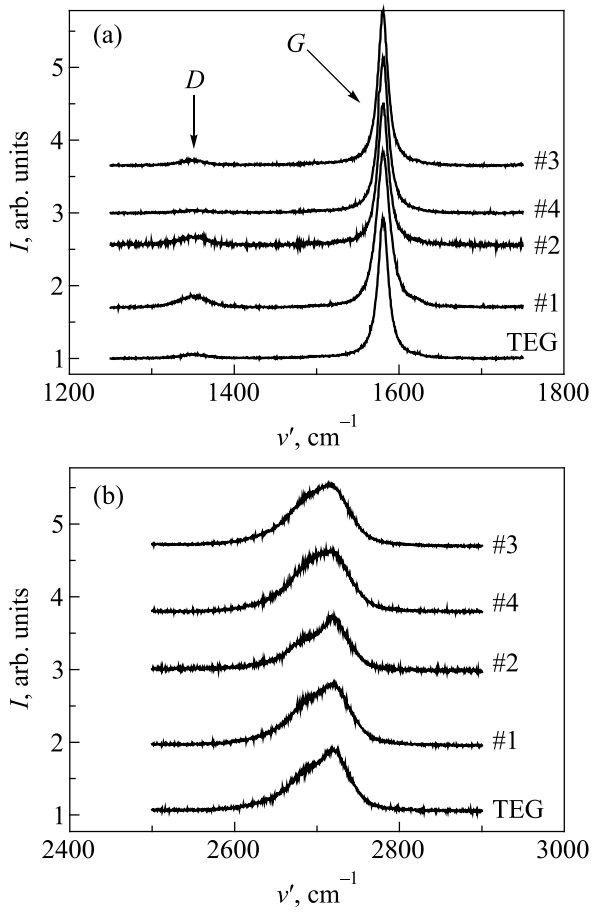

Fig. 2. Fragments of Raman spectra of TEG and GNPs obtained by chemical method (#1) and sonication in ethanol (#2), in acetone (#3) and in water (#4): D band and G band (a), G' band (b).

and overtones of D band. However, the exact position of each band and its shape, as well as the ratio of the integral intensity of the G band and D band for each specimen, are significantly different.

In the Raman spectrum of source TEG there is an intensive G band. The intensity of the D band is very small. The half-width of G band is 15 cm^{-1}. This value is close to the value of G line half-width for high-oriented pyrolytic graphite (HOPG). The Raman spectrum for source TEG also contains the wide band around 2700 cm^{-1} called the G' band and attributed to the D band's overtone. This band is not symmetric and is a combination of two bands (G_1' and G_2'). Significant broadening of the G' band and the presence of the shoulder on the right side point out on a multilayer structure of TEG.

For the specimen obtained by the treatment of source TEG with $KMnO_4$ solution in sulphuric acid (specimen #1), the essential increase of D band intensity compared to the source TEG is observed. Such increasing in D line intensity as well as broadening of the G band (up to 18 cm^{-1}) reflect significant growth of graphite layer structure defectiveness and possible re-hybridization of carbon atoms from sp^2 to sp^3 state. The G band for sample #1 is slightly shifted to longer wavelengths, which indicates a decrease in the number of layers in these GNPs.

Among all specimens obtained by sonication of TEG, the greatest value A_G/A_D is observed for specimen #2 (sonication in ethanol). For the other two specimens, this ratio is close to the corresponding value in source TEG. The broadening of the G band for these specimens is also significantly smaller compared to specimen #1 and close to the broadening of the G band in the source TEG. Thus, according to the Raman spectroscopy data, the graphite layers' defectiveness for the sonicated specimens is significantly smaller compared to specimen #1. As for the number of graphite layers in the sonicated specimens, the G' band's significant broadening indicates their multilayered structure. The structure of the investigated GNPs specimens has been studied in more detail in paper [16].

2.3. Measurements of resistance in a magnetic field

For resistance measurements, the bulk specimens from GNPs powders have been prepared by a cold-pressing method using a polyvinyl acetate adhesive. GNPs powders have been mixed with an aqueous solution of polyvinyl acetate. The obtained mixture was sonicated for 30 minutes and dried for constant mass. The mass part of polyvinyl acetate in the dry mixture was 25 %. Then dry mixture has been pressed at room temperature, and bulk specimens in the form of rectangular parallelepipeds (1 × 3.5 × 15 mm) have been made. The density of prepared bulk GNPs specimens is about 1.7 g/cm^3. Note that, in samples with a density of more than 0.8 g/cm^3, graphite nanoplatelets are orderly oriented due to uniaxial compression so that a layered structure perpendicular to the compression axis is formed in the samples.

The resistivity and magnetoresistance of bulk GNPs have been measured by a standard four-probe DC compensation method in the temperature range from 4.2 K to 293 K and in a magnetic field up to 2.2 T directed perpendicular to the current flowing through the specimen. The magnetoresistance $\Delta\rho/\rho_0$ is determined by the ratio of $\Delta\rho = (\rho(B) - \rho_0)/\rho_0$, where $\rho(B)$ and ρ_0 are the resistances in the magnetic field with induction B and in zero magnetic field, respectively. The error of the resistance measurements did not exceed 0.5 %.

3. Resistivity of bulk specimens of graphite nanoplatelets

Figure 3 presents the temperature dependence of resistivity for bulk specimens obtained by chemical treatment and by sonication of the initial TEG. The temperature dependence of resistivity for the source TEG is also shown in Fig. 3 for comparison.

Figure 3 shows that for all bulk specimens made of GNPs, as for the source TEG, decreasing temperature dependence of resistivity is observed. Before proceeding to a more detailed analysis of the temperature dependence, we note that as it is known, the resistance of bulk pressed specimen is determined by two terms $R = R_p + R_c$, where R_p is the resistance of individual particles, and R_c is the contact resistance between particles. In turn, the contact resistance R_c depends on the contact spot size and the contact pressure. The last two parameters (size of the contact spot and the contact pressure) largely depend on the value of the particle's linear expansion temperature coefficient. For specimens with a low mass content of binder, the effect of the binder on the contact resistance between the individual particles is negligibly small. Thus, the character of the resistivity temperature dependence for the bulk specimen reflects the resistance temperature dependence for individual GNP.

As can be seen from Fig. 3, the temperature coefficient of resistance α is approximately the same for all GNPs bulk specimens and its value is close to the corresponding value of α for the source TEG. Such resistivity temperature dependence is typical of graphite with a crystallite size less than 100 nm. It is due, on the one hand, to an increase in the charge carrier's concentration with a temperature for $T > 50$ K, and on the other hand, to a weak dependence of charge carrier mobility on temperature under prevailing charge carriers scattering at crystalline boundaries [17].

However, in the low-temperature range, there are significant differences in the resistivity dependences for GNPs obtained by different methods. For bulk specimens of GNPs obtained by sonication of source TEG in different liquids as well as for the initial TEG at low temperatures, resistivity does not depend on temperature. This is a consequence of the existence of a slight overlap of the valence band and conduction band in graphite materials, which leads to the fact that the concentration of charge carriers remains constant at low temperatures. This effect is typical of high-oriented pyrolytic graphite and natural dispersed graphite with moderate crystalline size. Instead, for GNPs prepared by chemical treatment of source TEG, there is an abnormal growth of resistivity at low temperature that cannot be explained in terms of classical conductivity mechanisms. A similar increase in resistance at low temperature has been found for fine crystalline pyrolytic graphite and multiwall carbon nanotubes with imperfect structure [18] and has been explained by the manifestation of effects of charge carrier's weak localization and interaction effects.

4. Magnetoresistance of thermoexfoliated graphite

Figure 4 presents the field dependence $\Delta\rho(B)/\rho_0$ for a bulk specimen of source TEG at two different temperatures, and the dependence $\Delta\rho/\rho_0$ on the square of magnetic field B^2 is shown on the inset.

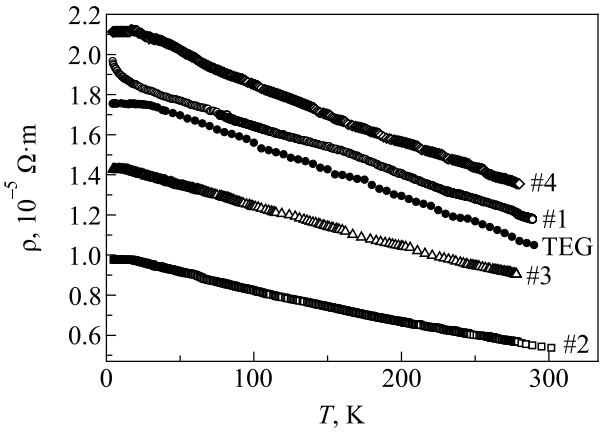

Fig. 3. Temperature dependences of resistivity for initial bulk TEG specimen, for GNPs obtained by chemical treatment (#1), and GNPs sonicated in: ethanol (#2), acetone (#3), water (#4).

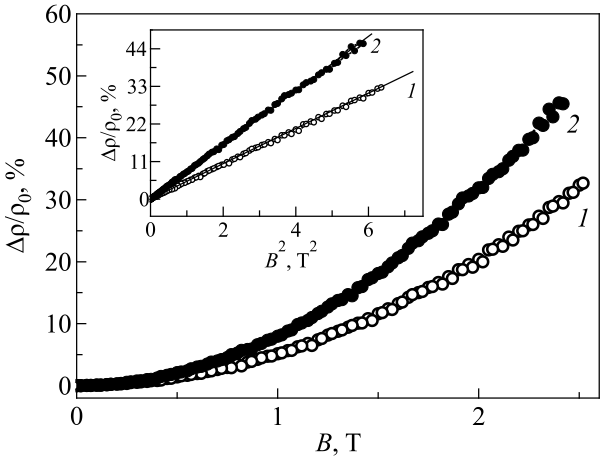

Fig. 4. Dependences $\Delta\rho(B)/\rho_0$ and $\Delta\rho(B^2)/\rho_0$ for TEG. $T = 293$ K (*1*) and $T = 77$ (*2*) K.

As shown in Fig. 4, $\Delta\rho/\rho_0$ is positive and quadratic with respect to the field for TEG. With decreasing temperature, the magnetoresistance increases and achieves the value ~ 45 % at $T = 77$ K.

This quadratic dependence of the resistance for single-crystal graphite on the magnetic field is usually described by the formula:

$$\frac{\Delta\rho}{\rho_0} = \frac{p}{n}\mu_p\mu_n B^2, \qquad (1)$$

where p and n are the concentration while μ_p and μ_n are the mobilities of holes and electrons, respectively. As the temperature decreases, the magnetoresistance increases because of a significant increase in the charge carrier's mobility. Moreover, at 4.2 K, magnetoresistance can reach several hundred percent. Thus, for TEG a typical, as for monocrystalline graphite, field and temperature dependence of magnetoresistance is observed. Under the assumption that $p/n = 1.2$ [19] the average values of mobility $\overline{\mu}_{n,p}$ estimated from Eq. (1) are 0.21 m^2/V·s at $T = 293$ K and 0.26 m^2/V·s at $T = 77$ K.

5. Magnetoresistance of graphite nanoplatelets prepared by chemical method

The dependences of magnetoresistance $\Delta\rho/\rho_0$ on magnetic field B for GNPs prepared by treatment of TEG by the solution of potassium permanganate in sulfuric acid (specimen #1) at two different temperatures are presented in Fig. 5.

Figure 5 shows that at room temperature, magnetoresistance is positive and quadratic with respect to the magnetic field according to the classical mechanism described by Eq. (1). The magnetoresistance changes sign and is negative at $T = 77$ K. However, the magnetoresistance retains a quadratic dependence on the magnetic field up to ~ 1.2 T.

As it is known for graphite materials with weak structure ordering, in particular, for fine crystalline anisotropic pyrolytic graphite [7], multiwall carbon nanotubes with imperfect structure [18, 20], and intercalated graphite compounds [21] at low temperatures, negative magnetoresistance is usually observed. This phenomenon is usually explained by the effect of the charge carriers' weak localization that occurs for systems with weak structural disordering. (The criterion for strong disordering is the relation $k_F \times \ell \sim 1$, where k_F is the Fermi wave vector, and ℓ is the electron mean free path [22].) The quantum correction to conductivity due to the weak localization effect depends on the system dimensionality and may be proportional to the magnetic induction's square root or logarithm. Another effect that occurs for weakly disordered systems is the effect of charge carriers' interaction. In contrast to the weak localization, this effect does not change the sign of magnetoresistance at low temperatures. Corrections to conductivity due to the charge carriers' localization are usually positive for the case of the weak spin-orbit interaction, i.e., the conductivity in the magnetic field increases, while the conductivity in the magnetic field due to the charge carriers' interaction decreases. Both the weak localization effects and the effects of the charge carriers' interaction depend on the degree of structural perfection of the graphite materials studied. For the systems with a sufficiently high defect density, the effects of weak localization predominate, which leads to negative magnetoresistance. For materials with less defectiveness, the effects of charge carriers' interaction, which do not change the sign of magnetoresistance, prevail in charge transport properties.

Figure 6 shows the experimental field dependence of relative correction to conductivity $(\sigma(B) - \sigma_0)/\sigma_0 = \Delta\sigma(B)/\sigma_0$ in magnetic field for a bulk specimen of GNPs obtained by chemical method. Dependence $\Delta\sigma(B^2)/\sigma_0$ is also shown in Fig. 6 (see inset).

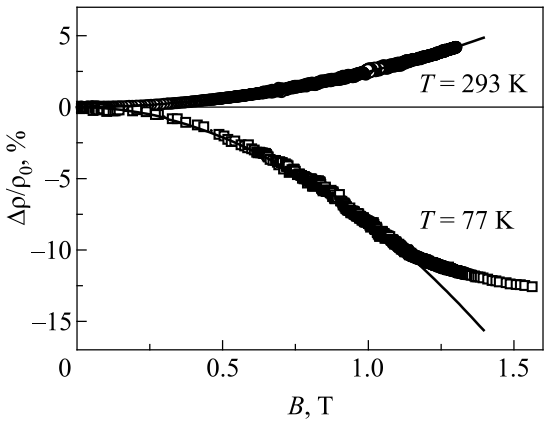

Fig. 5. Dependence $\Delta\rho(B)/\rho_0$ for specimen #1 at $T = 293$ K and at $T = 77$ K. Solid lines are approximations by dependence $\Delta\rho/\rho_0 \propto k \times B^2$ with different coefficients k.

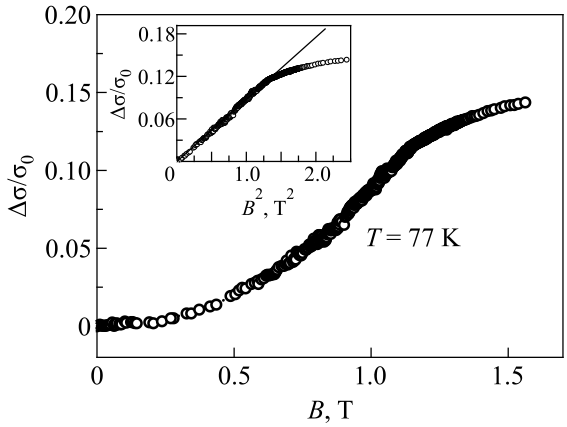

Fig. 6. Dependences of relative addition to conductivity $\Delta\sigma/\sigma_0$ on magnetic field B and square of magnetic field B^2 (inset) for a bulk specimen of chemically obtained GNPs.

As can be seen from Fig. 6, the experimental dependence $\Delta\sigma(B)/\sigma_0$ up to 1.2 T may be approximated by a quadratic dependence $\Delta\sigma/\sigma_0 = cB^2$, $c = 0.09\cdot T^{-2}$. Above this field, the deviation from the quadratic dependence takes place.

Thus, for chemically obtained GNPs, we observe: (i) according to structural investigations, significant structure distortions in comparison with the source TEG. In particular, a decrease in the size of the crystallites both along the graphite planes and along the *c* axis; (ii) anomalous low-temperature increase in resistance; and (iii) low-temperature increase in conductivity in the magnetic field. Analyzing these facts, we can assume that for this specimen of GNPs at low temperatures, the effect of weak localization and the charge carriers interaction take place.

GNPs can be considered as 2D systems. For 2D systems, relative correction to conductivity in magnetic fields due to charge carriers' weak localization effect is determined as [23–25]:

$$\frac{\Delta\sigma_{\text{loc}}}{\sigma_0} = \begin{cases} \dfrac{e^2}{2\pi^2\hbar\sigma_{20}}\dfrac{2e^2D^2\tau_\varphi^2}{3\hbar}B^2 = c_{\text{loc}}B^2, & B < \dfrac{\hbar}{4eD\tau_\varphi}; \\ \dfrac{e^2}{2\pi^2\hbar\sigma_{20}}\ln\left(\dfrac{4eD\tau_\varphi}{\hbar}B\right), & B > \dfrac{\hbar}{4eD\tau_\varphi}, \end{cases} \tag{2}$$

where D is the electron diffusion coefficient, τ_φ is the wave function phase relaxation time. Diffusion coefficient D can be written as:

$$D = \frac{L_T^2 k_B T}{\hbar}, \tag{3}$$

where L_T is the wave function thermal coherence length. In the first approximation, as L_T we will consider the size of crystallites along graphite planes L. For specimen #1, this size is about 4 nm. The characteristic field of weak localization is:

$$B^*_{\text{loc}} = \frac{\hbar}{4eD\tau_\varphi}. \tag{4}$$

So, when the magnetic field is below B^*_{loc}, correction to the conductivity is positive and proportional to the square of the magnetic field; when the magnetic field is above B^*_{loc}, correction is positive and proportional to the logarithm of the magnetic field.

As shown in Fig. 6, the magnetic field at which the character of dependence $\Delta\sigma(B)/\sigma_0$ changes is ~ 1.2 T. Apparently, this magnetic field can be considered as the characteristic field B^*_{loc}. Using Eqs. (3) and (4), we can estimate the value of the electron wave function phase relaxation time τ_φ at $T = 77$ K, getting the value $\tau_\varphi = 8.2\cdot10^{-13}$ s. We rewrite the coefficient c_{loc} at B^2 (Eq. 2) using the expression for two-dimensional conductivity σ_{20} for weakly disordered graphite:

$$\sigma_{20} = \frac{\Delta E_F e^2 L}{\sqrt{3}\pi\hbar a_0\gamma_0}, \tag{5}$$

where a_0 is the primitive translation vector for graphene layer, $a_0 = 0.246$ nm, γ_0 is the overlap integral for neighboring carbon atoms in the graphene layer, ΔE_F is the shift of Fermi energy to the valence band. Taking into account Eqs. (2), (3), and (5), c_{loc} can be rewritten as:

$$c_{\text{loc}} = \frac{\sqrt{3}e^2\tau_\varphi^2\gamma_0 L^3 k_B^2 T^2 a_0}{3\pi\hbar^4\Delta E_F}. \tag{6}$$

Comparing the experimentally determined value of c (Fig. 6) and Eq. (6) for c_{loc}, we can estimate the shift of Fermi energy to the valence band. The calculated value is $\Delta E_F = 0.02$ eV. This value of Fermi energy shift correlates well with the corresponding value in fine crystalline graphite or multiwall carbon nanotubes with imperfect structure [20].

Thus, for GNPs obtained by chemical treatment of source TEG with the potassium permanganate solution in sulfuric acid, the negative magnetoresistance is observed, which is explained by the manifestation of the charge carrier's weak localization effect. This effect is caused by a high degree of defectiveness of GNPs obtained by this method.

6. Magnetoresistance of graphite nanoplatelets prepared by sonication method

Figure 7 presents the dependences of magnetoresistance $\Delta\rho/\rho_0$ on magnetic field B at two temperatures for GNPs specimens prepared by sonication treatment of source TEG in ethanol [Fig. 7(a)], acetone [Fig. 7(b)], and water [Fig. 7(c)]. Also, dependences $\Delta\rho(B^2)/\rho_0$ for all specimens are given on the insets.

As shown in Fig. 7 for GNPs prepared by sonication method, the character of dependence $\Delta\rho(B)/\rho_0$ is essentially different from both the source TEG (Fig. 4) and chemically prepared GNPs (Fig. 5). For the source TEG, magnetoresistance remains positive even at low temperatures. However, for GNPs prepared by the sonication method, the dependence of magnetoresistance on temperature is negligible. Of course, such temperature independence of the magnetoresistance could be explained by the temperature independence of the charge carriers' mobility at the predominant crystallite boundary charge carriers' scattering. However, since the crystallites' sizes for the source TEG and for prepared by sonication method GNPs do not differ significantly, this explanation does not seem plausible. Another feature for the $\Delta\rho(B)/\rho_0$ dependence is that starting from the magnetic field ~ 0.8 T, not a "classical" quadratic relative to a magnetic field, but a linear dependence $\Delta\rho(B)/\rho_0$ is observed.

Thus, for obtained by sonication method GNPs specimens, there are two unusual peculiarities: independence of magnetoresistance on temperature and linear dependence of magnetoresistance on the magnetic field starting from ~ 0.8 T.

As is known, the magnetoresistance linear with respect to the magnetic field was first found for some semiconductors with a zero bandgap, in particular in silver chalcogenides [26–30], epitaxial layered InSb structures [31], disordered

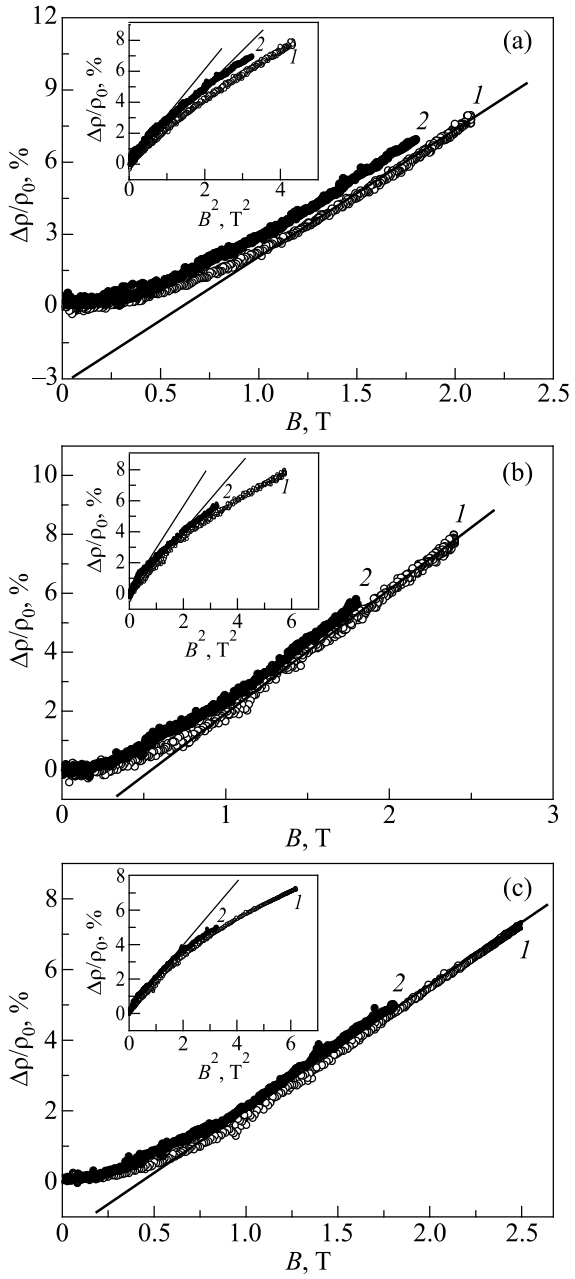

Fig. 7. Dependences $\Delta\rho(B)/\rho_0$ and $\Delta\rho(B^2)/\rho_0$ (inset) for GNPs' specimens after sonication in ethanol (a), acetone (b), and water (c), T, K: 293 (*1*), 77 (*2*).

semiconductors such as MnAs–GaAs [32], etc. There are two types of linear magnetoresistance.

In the classical case, linear magnetoresistance is observed in structures that contain either clusters with significantly different conductivities or big pores. Obviously, these properties are not characteristic of the investigated GNPs.

Another case of quantum linear magnetoresistance is considered in works by Abrikosov.

According to the model proposed by Abrikosov, the magnetoresistance is linearly proportional to the magnetic field even at relatively small magnetic fields. Abrikosov's magnetoresistance is positive, does not reach saturation and does not depend on temperature [33–35].

Necessary conditions for the implementation of the quantum linear magnetoresistance effect are the layered structure of the material with weak interaction between the layers and the quasilinear energy dispersion law. This quantum effect becomes significant only when the individual Landau levels associated with the electronic orbits are allowed, that is $\hbar\omega_c > k_BT$, and in relatively strong magnetic fields, where $\hbar\omega_c > E_F$. Thus, electrons are on the lowest quantum level, and a quantum limit can be achieved.

Let us analyze whether these conditions are realized for the studied GNPs.

Graphite nanoplatelets, like any anisotropic graphite, have a layered structure. The covalent bonds in the graphene layer are almost ten times stronger than the weak Van der Waals bonds between the graphene layers. According to structural studies [16], the sonication does not cause significant defects in the graphene layers themselves. However, the result of such sonication in different liquids is the weakening of the bonds between the graphene layers.

It is obvious that the weakening of Van der Waals interaction between graphene layers enhances the structural anisotropy and anisotropy of conductivity, which allows one to consider GNPs as a two-dimensional structure, while two-dimensional graphite is indeed characterized by a linear energy dispersion law.

Let's consider the conditions for observing the linear magnetoresistance in GNPs' specimens. The first condition is $\hbar\omega_c > k_BT$, where ω_c is the cyclotron frequency, $\omega_c = eB/m^*$, m^* is the charge carriers' effective mass. Since the effective mass of the charge carriers for graphite is exceedingly small, this condition is satisfied starting from relatively small magnetic fields ~ 2.2 T, even at room temperature. At $T = 77$ K, linear magnetoresistance can be observed from a magnetic field ~ 0.6 T. Thus, at the temperatures and magnetic fields at which the magnetoresistance research was conducted, the observation of the linear magnetoresistance is quite possible.

As for the second condition $\hbar\omega_c > E_F$, it is necessary to estimate the shift of the Fermi energy E_F to the valence band for obtained GNPs.

As is known for monocrystalline hexagonal graphite, there is a small overlap E_0 between the valence band and the conduction band, $E_0 = 40$ meV. In this case, both electrons and holes are intrinsic charge carriers; their concentration for monocrystalline hexagonal graphite is equal. The Fermi level is strictly in the middle of the overlap of the valence band and the conduction band. For partially graphitized materials, for example, for fine crystalline anisotropic graphite, the overlap of the valence band and the conduction band decreases; thus, the Fermi energy level is slightly shifted towards the valence band. For the turbostratic graphite as well as for two-dimensional graphite, there is only slight touching between the valence band and the conduction band, and the Fermi energy level is shifted to the valence band.

Consider the possible mechanisms of magnetoresistance in the investigated specimens of GNPs in a small magnetic field, where the quadratic relative to the magnetic field dependence of magnetoresistance is observed. From the analysis of the structure parameters of GNPs prepared by the sonication method and the absence of magnetoresistance temperature dependence, we can assume that the quadratic relative to magnetic field magnetoresistance dependence is associated with the effect of charge carrier's interaction. As mentioned above, this effect is observed for weakly ordered systems with a sufficiently high concentration of charge carriers and a small degree of defectiveness.

The relative addition to the conductivity in the magnetic field associated with the manifestation of the effect of the charge carrier's interaction for the two-dimensional case is defined by the formulae [23–26]:

$$\frac{\delta\sigma_{\text{int}}}{\sigma_0} = \begin{cases} \dfrac{e^2}{2\pi^2\hbar\sigma_0} G(T,B) \dfrac{1.2e^2D^2}{\pi^2 k_B^2 T^2} B^2 = c_{\text{int}} B^2, \ B < \dfrac{\pi k_B T}{2eD}; \\ \dfrac{e^2}{2\pi^2\hbar\sigma_0} G(T,B) \ln\left(\dfrac{2eD}{\pi k_B T} B\right), \ B > \dfrac{\pi k_B T}{2eD}, \end{cases} \tag{7}$$

where $G(T, B)$ is the charge carriers interaction parameter (in the general case, G is the function of temperature and magnetic field); however, at low enough temperatures and small magnetic fields, G is a constant, and for it, the ratio $G << 1$ is true. The characteristic interaction field can be written as:

$$B^*_{\text{int}} = \frac{\pi k_B T}{2eD}. \tag{8}$$

To estimate the value of the characteristic field B^*_{int}, we use Eq. (3) for the diffusion coefficient D. As a first approximation, we assume that $L_T = L$, where L is the mean crystallite size for GNPs prepared by the sonication method. In doing so, we obtain the calculated characteristic interaction field $B^*_{\text{int}} = 0.65$ T. In this case, for magnetic fields, less than 0.65 T, the relative addition to the conductivity associated with the effect of the charge carriers' interaction is negative and quadratic in the field. For magnetic fields above 0.65 T, the relative addition to the conductivity is negative and proportional to the magnetic field logarithm.

For magnetic fields B below the characteristic interaction field B^*_{int} we can rewrite the expression (7) for relative addition to conductivity using Eq. (5) for 2D conductivity:

$$\frac{\delta\sigma_{\text{int}}}{\sigma_0} = \frac{0.6\sqrt{3}Ge^2L^3\gamma_0 a_0}{\pi^3\hbar^2\Delta E_F} B^2 = c_{\text{int}} B^2. \tag{9}$$

Note that according to Eq. (9), the coefficient c_{int} at B^2 does not depend on the temperature that is observed experimentally.

Figure 8 presents the experimental dependences of relative additions to conductivity in a magnetic field $(\sigma(B) - \sigma_0)/\sigma_0 = \Delta\sigma(B)/\sigma_0$ for GNPs specimens prepared by the sonication method.

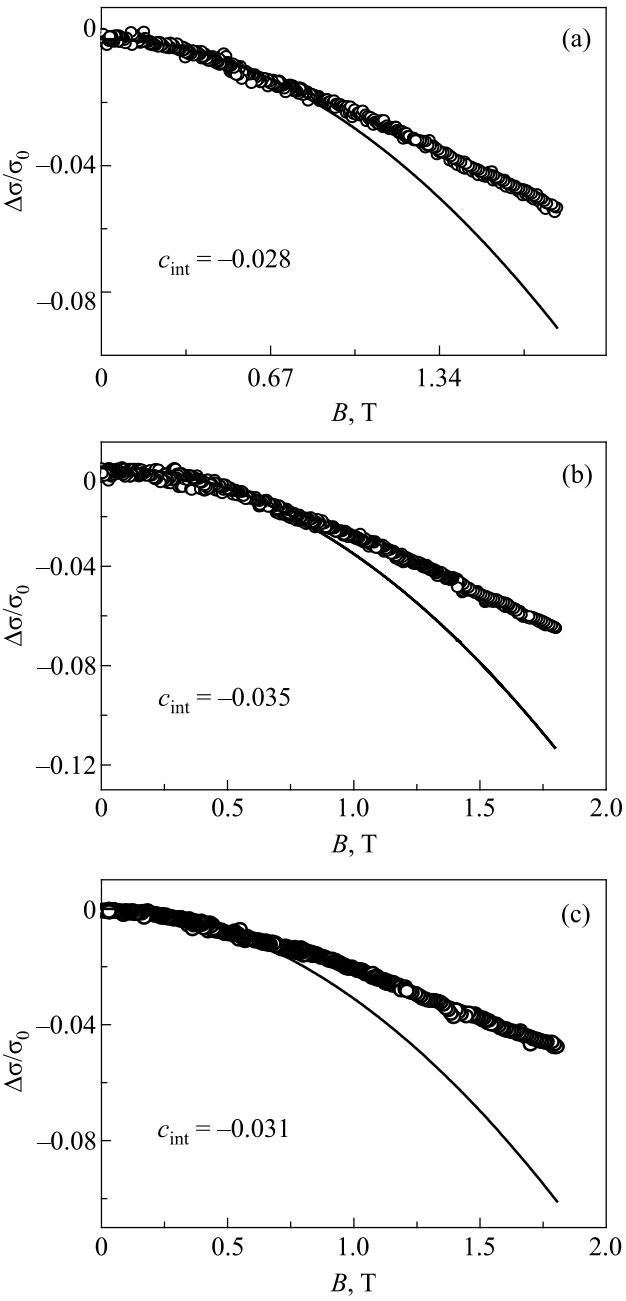

Fig. 8. Experimental dependences $\Delta\sigma(B)/\sigma_0$ at $T = 77$ K for specimens of GNPs, sonicated in ethanol (a), acetone (b), and water (c). Solid line is approximation by the dependence (9) of type $\Delta\sigma(B)/\sigma_0 = c_{\text{int}} \times B^2$. The value of c_{int} for each GNPs specimen is indicated in the Figures.

Using the values of the coefficients c_{int} obtained from the experimental $\Delta\sigma(B)/\sigma_0$ dependences according to Eq. (9), the Fermi energy shift ΔE_F for each specimen of GNPs has been estimated. The obtained values of ΔE_F are respectively ~ 0.013 eV for GNPs prepared by sonication in ethanol, ~ 0.010 eV for GNPs prepared by sonication in acetone and ~ 0.011 eV for GNPs prepared by sonication in water. Therefore, the condition $\hbar\omega_c > \Delta E_F$ for observing the linear magnetoresistance is fulfilled above magnetic field ~ 0.6 T.

Conclusions

The undertaken research has shown that magnetoresistance of GNPs is very sensitive to the degree of defectiveness of their structure. It has been established that magnetoresistance is negative for GNPs, prepared by chemical treatment of source TEG with strong oxidants, such as a solution of potassium permanganate in sulfuric acid in the magnetic field range up to 2.2 T. This negative magnetoresistance is associated with the manifestation of the charge carriers' weak localization in systems with structure imperfections. It is shown that the magnetoresistance in the above-mentioned magnetic field interval is positive for GNPs produced by the sonication method. When the magnetic field is below ~ 0.7 T, magnetoresistance can be described by the charge carriers' interaction model. Above 0.7 T, we observe the magnetoresistance, which is linear relative to a magnetic field and independent of temperature. This case can be explained in terms of Abrikosov's model of quantum linear magnetoresistance.

We believe that for GNPs obtained by chemical treatment of source TEG, quantum linear magnetoresistance should also be observed, but starting with higher values of the magnetic field. Indeed, these GNPs, like all graphite materials, have a layered structure with a weak interaction between the layers and a linear dispersion ratio near the corners of the Brillouin zone. Condition $\hbar\omega_c > k_B T$ for chemically split graphite materials is also valid, as for other graphite structures with an abnormally small value of the charge carrier's effective mass. The condition $\hbar\omega_c > E_F$ for graphite materials with a high degree of defectiveness, for which the Fermi energy level is significantly shifted to the valence band due to the higher concentration of holes compared to the electron concentration, according to our estimates, begins to be fulfilled for magnetic fields ~ 2.5 T.

Acknowledgments

This work was partly supported by the NATO for Peace Programme, project G5697 "Globular Carbon based Structures and Metamaterials for Enhanced Electromagnetic Protection" (CERTAIN).

1. A. A. Bright, *Phys. Rev. B* **20**, 5142 (1979).
2. C. Auache, *Physica B+C* **99**, 509 (1980).
3. Y. Hishiyama, S. Mrozowski, and A. S. Vagh, *Carbon* **9**, 367 (1971).
4. Y. Hishiyama, *Carbon* **8**, 259 (1970).
5. P. Delhaes, *Chem. Phys. Carbon* **7**, 193 (1971).
6. L. D. Woolf, H. Ikezi, and Y. R. Lin-Liu, *Solid State Commun.* **54**, 49 (1985).
7. L. Y. Matzui and Ye. I. Kharkov, *Fiz. Nizk. Temp.* **9**, 760 (1983) [*Low Temp. Phys.* **9**, 389 (1983)].
8. Y. Koike, S. Morita, T. Nakanonuyo, and T. Fukase, *J. Phys. Soc. Jpn.* **54**, 713 (1985).
9. V. Bayot, L. Piraux, and J. P. Issi, *Phys. Rev. B* **40**, 3514 (1989).
10. Ram Sevak Singh, Xiao Wang, Wei Chen, Ariando, and A. T. S. Wee, *Appl. Phys. Lett.* **101**, 183105 (2012).
11. W. J. Wang, K. H. Gao, Z. Q. Li, T. Lin, J. Li, C. Yu, and Z. H. Feng, *Appl. Phys. Lett.* **105**, 182102 (2014).
12. M. Gryglas-Borysiewicza, B. Jouaulta, J. Tworzydłod, S. Lewinskaa, W. Strupinskie, and J. M. Baranowski, *Transport Properties of Disordered Graphene Layers*, *Proceedings of the XXXVIII International School and Conference on the Physics of Semiconductors "Jaszowiec"*, *Acta Phys. Pol. A* **116**, 838 (2009).
13. A. L. Friedman, J. L. Tedesco, P. M. Campbell, J. C. Culbertson, E. Aifer, F. K. Perkins, R. L. Myers-Ward, J. K. Hite, C. R. Eddy, G. G. Jernigan, and D. K. Gaskill, *Nano Lett.* **10**, 3962 (2010).
14. X. Zhang, Q. Z. Xue, and D. D. Zhu, *Phys. Lett. A* **320**, 471 (2004).
15. Yu. S. Perets, I. V. Ovsiienko, L. L. Vovchenko, L. Yu. Matzui, O. A. Brusilovetz, and I. P. Pundyk, *Ukr. J. Phys.* **57**, 219 (2012).
16. I. Ovsiienko, T. Len, L. Matzui, O. Lazarenko, and F. Le Normand, *Ukr. J. Phys.* **63**, 759 (2018).
17. I. Ovsiienko, L. Matzui, I. Berkutov, I. Mirzoiev, T. Len, Yu. Prylutskyy, O. Prokopov, and U. Ritter, *J. Mater. Sci.* **53**, 716 (2018).
18. I. V. Ovsienko, L. Y. Matzui, I. V. Yatsenko, S. V. Khrapatiy, Y. I. Prylutskyy, U. Ritter, P. Scharff, and F. Le Normand, *Mat.-wiss. u Werkstofftech.* **44**, 161 (2013).
19. L. Y. Matzui, I. V. Ovsiienko, and L. L. Vovchenko, *Fiz. Nizk. Temp.* **27**, 68 (2001) [*Low Temp. Phys.* **27**, 52 (2001)].
20. I. Ovsiienko, T. Len, L. Matzui, V. Tkachuk, I. Berkutov, I. Mirzoiev, Yu. Prylutskyy, N. Tsierkezos, and U. Ritter, *Mat.-wiss. u Werkstofftech.* **47**, 254 (2016).
21. V. Ya. Tkachuk, I. V. Ovsiyenko, L. Yu. Matzui, T. A. Len, Yu. I. Prylutskyy, O. A. Brusylovets, I. B. Berkutov, I. G. Mirzoiev, and O. I. Prokopov, *Mol. Cryst. Liq. Cryst.* **639**, 137 (2016).
22. B. I. Belevtsev, E. Yu. Belyaev, Yu. F. Komnik, and E. Yu. Kopeichenko, *Fiz. Nizk. Temp.* **23**, 965 (1997) [*Low Temp. Phys.* **23**, 724 (1997)].
23. B. L. Altshuler, D. E. Khmel'nitzkii, A. I. Larkin, and P. A. Lee, *Phys. Rev. B* **22**, 5142 (1980).
24. B. L. Altshuler and A. G. Aronov, *Solid State Commun.* **46**, 429 (1983).
25. B. L. Altshuler, A. G. Aronov, A. I. Larkin, and D. E. Khmel'nitzkii, *Sov. Phys. JETP* **54**, 411 (1981).
26. Xiao-Lin Wang, Shi Xue Dou, and Chao Zhang, *NPG Asia Mater.* **2**, 31 (2010).
27. M. Lee, T. Rosenbaum, M. Saboungi, and H. Schnyders, *Phys. Rev. Lett.* **88**, 066602 (2002).
28. M. Kreutzbruck, G. Lembke, B. Mogwitz, C. Korte, and J. Janek, *Phys. Rev. B* **79**, 035204 (2009).
29. R. Xu, A. Husmann, T. F. Rosenbaum, M. L. Saboungi, J. E. Enderby, and P. B. Littlewood, *Nature* **390**, 57 (1997).

30. I. Ovsiienko, T. Len, L. Matzui, O. Golub, Yu. Prylutskyy, and P. Eklund, *Mater. Sci. Eng. C* **26**, 1180 (2006).
31. I. Ovsiienko, L. Matzui, T. Len, N. Zakharenko, N. Babich, Yu. Prylutskyy, D. Hui, Y. Strzhemechny, and P. Eklund, *Nanoscale Res. Lett.* **3**, 60 (2008).
32. H. Johnson, S. Bennett, R. Barua, L. Lewis, and D. Heiman, *Phys. Rev. B* **82**, 085202 (2010).
33. A. Abrikosov, *Phys. Rev. B* **58**, 2788 (1998).
34. A. Abrikosov, *Europhys. Lett.* **49**, 789 (2000).
35. A. Abrikosov, *Phys. Rev. B* **60**, 4231 (1999).

Магнітоопір графітових нанопластинок з різною структурою

I. V. Ovsiienko, T. A. Len, O. A. Syvolozhskyy, L. Yu. Matzui, I. G. Mirzoiev, V. V. Andrievskii, E. Yu. Beliayev

Досліджено магнітоопір об'ємних зразків графітових нанопластинок, отриманих різними методами, в магнітних полях до 2,2 Тл. Для графітових нанопластинок, приготованих хімічною обробкою вихідного графіту розчином перманганату калію в сірчаній кислоті, магнітоопір є від'ємним. Цей від'ємний магнітоопір можна пояснити з погляду моделі слабкої локалізації носіїв заряду в системі з недосконалою структурою. Для графітових нанопластинок, отриманих методом ультразвукової обробки, магнітоопір є додатним і не залежить від температури. Більш того, в магнітному полі понад ~ 0,7 Тл магнітоопір є лінійним щодо магнітного поля. Показано, що лінійний магнітоопір можна пояснити з погляду квантового лінійного магнітоопору моделі Абрикосова.

Ключові слова: графітові нанопластинки, магнітоопір, досконалість структури, слабка локалізація, квантовий магнітоопір.